Appl. Math. J. Chinese Univ.
2023, 38(3): 373-391

Flow and heat transfer of a nanofluid through a porous medium due to stretching/shrinking sheet with suction, magnetic field and thermal radiation

Ubaidullah Yashkun[1,2] Khairy Zaimi[1,*] Suliadi Firdaus Sufahani[3]
Mohamed R. Eid[4,5] Mohammad Ferdows[6]

Abstract. This study investigates the suction and magnetic field effects on the two-dimensional nanofluid flow through a stretching/shrinking sheet at the stagnation point in the porous medium with thermal radiation. The governing partial differential equations (PDEs) are converted into ordinary differential equations (ODEs) using the similarity transformation. The resulting ODEs are then solved numerically by using the bvp4c solver in MATLAB software. It was found that dual solutions exist for the shrinking parameter values up to a certain range. The numerical results obtained are compared, and the comparison showed a good agreement with the existing results in the literature. The governing parameters' effect on the velocity, temperature and nanoparticle fraction fields as well as the skin friction coefficient, the local Nusselt number and the Sherwood number are represented graphically and analyzed. The variation of the velocity, temperature and concentration increase with the increase in the suction and magnetic field parameters. It seems that the thermal radiation effect has increased the local Sherwood number while the local Nusselt number is reduced with it.

§1 Introduction

The study of hydrodynamic flow and heat transfer through a stretching/shrinking sheet received keen observation by many researchers due to its emerging applications in engineering and manufacturing processes. The applications are in hot rolling, cooling of electronic devices, and nuclear reactors as well as in the hydrodynamics process (see Ibrahim et al. [1]). Sakadias [2] was the first to initiate the investigation of the laminar boundary layer flow of a viscous

Received: 2020-05-17. Revised: 2021-08-20.
MR Subject Classification: 35Q79, 80A21, 76S05, 34B15.
Keywords: stagnation point flow, nanofluid, porous medium, suction, magnetohydrodynamic, thermal radiation.
Digital Object Identifier(DOI): https://doi.org/10.1007/s11766-023-4150-9.
The authors would like to acknowledge the support from the Fundamental Research Grant Scheme (FRGS) under a grant number of FRGS/1/2018/STG06/UNIMAP/02/3 from the Ministry of Education Malaysia.
*Corresponding author

and incompressible fluid on continuous solid surfaces. The flow through a stretching sheet is carried by Crane [3] and it produces a similar solution with the Heimenz boundary layer flow at the stagnation point. The study of flow on stagnation-point attracted the researchers due to its intensive and potential applications in the field of manufacturing processes, for example, aerodynamic, the extrusion of a plastic sheet, in addition to the cooling/drying of papers and textiles (Ishak et al. [4]; Kamal et al. [5]). Kamal et al. [5] investigated the stagnation-point flow and heat transfer through a stretching/shrinking sheet along with viscous dissipation and heat source/sink. They determined physically the stability of the first solution while the second solution is not stable. The quality of the final product of the manufacturing products depends on the skin friction coefficients, rate of heat transfers, and volume fraction. The study of stagnation point flow in two-dimension (2D) is carried out first by Hiemenz [6] by reducing the Navier-CStokes equation into ODEs using similarity transformations. After that, a number of researchers investigated the stagnation point flow toward the stretching sheet by using different physical effects as in Mahapatra and Gupta [7], Pop et al. [8], Nazar et al. [9], Hamid et al. [10] and recently by Yashkun et al. [11]. Different types of fluids like Casson fluid, Jeffery fluid and hybrid nanofluid are studied in [12–17]. The conventional base fluids such as water, oil, and ethylene glycol are poor heat transfer fluids due to their low thermal conductivity. To enhance the heat transfer, Choi [18] proposed for the first time a new type of fluid called nanofluid by suspending metallic nanoparticles into the base fluid. The nanofluids are the nanometer-sized particles dispersed into a base fluid. It is noted that the Thermal conductivity is effectively enhanced in the range of 15% - 40% as compared to the base fluid (Reddy and Shankar [19]). The magnetohydrodynamic (MHD) has numerous applications in the area of engineering and physics such as the petroleum process, MHD generators, nuclear reactors, aerospace, superconductors, and microfluidics (see Chaudhary et al. [20]). In microfluidics, MHD maintains to pump, confine and control liquid metals and ionized gases. The unsteady MHD flow and heat transfer through a permeable surface with suction or injection was investigated by Choudhary et al. [20]. They noticed that the velocity, temperature, and rate of heat transfer profiles decrease with an increase of the suction/injection parameter. The MHD has a significant role in the flow of fluids and has numerous applications in medicine, nuclear reactors, MHD generators, petroleum refining, and astrophysics. The MHD stagnation point flow over a stretching sheet was examined by Ishak et al. [21]. They determined that an increase in the heat transfer rate on the surface by the magnetic parameter as the free stream velocity is more than the stretching velocity. Suction has numerous applications in aerodynamics and space sciences as stated by Uwanta and Hamza [22]. They investigated the effect of suction/injection by thermal diffusion on unsteady hydromagnetic natural convection flow of viscous reactive fluid between two vertical porous plates. Ishak et al. [4] studied the effects of suction/injection through a vertical wall with heat flux on the laminar mixed convection boundary layer. They noticed that the suction/injection of fluid flow via a bounding surface, may substantially change the flow field and affect the heat transfer rate of the plate. Generally, suction can increase skin friction and heat transfer coefficients. The multiple solutions which cannot be seen experimentally therefore

numerical analysis of the fluid flow problems for such type of solutions is important Lund et al. [23–25], Rohni [26] and Dero et al. [27]. In addition, many further studies claimed that these solutions occur due to the existence of nonlinearity in equations of the fluid model and depend on the values of the physical parameters considers. The importance and applications of multiple solutions have been investigated by many researchers. However, the multiple solutions can help in developing the industry's alternative flow capability in emergency Lund, et al. [14]. Khashiie, et al. [28] investigated the magnetohydrodynamics (MHD) flow and heat transfer characteristics of a dual stratified micropolar fluid over a permeable stretching/shrinking sheet. They found that both assisting and opposing buoyancy flows have dual similarity solutions within a specific range of suction and stretching/shrinking parameters. Their findings show that the first solution is the real solution, whereas the second solution is not real (not stable). This study is the extension of Khan and Pop [29] with the addition of suction, MHD, and thermal radiation effect in a nanofluid. This paper aims to provide a comprehensive study of the two-dimensional boundary layer stagnation point flow of a viscous and incompressible fluid over a stretching/shrinking sheet in the presence of suction, MHD, and thermal radiation effects. Also, it is good to note that no exactly similar works to the present study have been found in the literature.

§2 Problem Formulation

Consider steady, two-dimensional and incompressible viscous flow of nanofluid over the stagnation point through a stretching/shrinking sheet with the plane $y = 0$. The flow is in the region $y > 0$. Along the $x - axis$ two equal and opposing forces are applied which caused the sheet to stretch or shrink while the origin is fixed, as demonstrated in Figure 1. The velocity distribution away from the stretching/shrinking sheet near the stagnation point is assumed as $u = u_e(x) = ax$ and $v = v_e(y) = -ay$, which is a positive constant. The ambient temperature and concentration are denoted by T_∞ and C_∞ when y tends to infinity. The governing

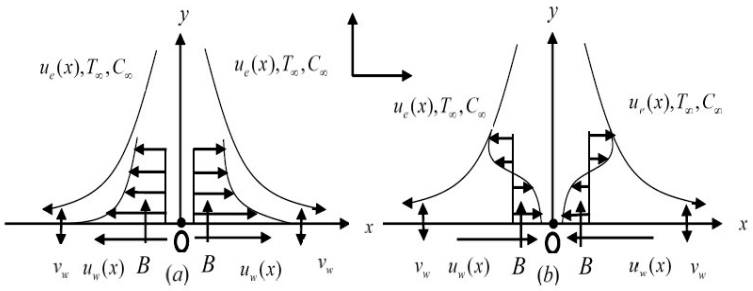

Figure 1. Physical model and coordinate system: (a) Stretching sheet and (b) Shrinking sheet.

equations for steady 2D stagnation point flow across a heated surface stretched/shrank through a permeable porous medium filled with a nanofluid as follows (see Mahapatra and Gupta [7]; Khan and Pop [29]; Nield and Kuznetsov [30])

$$\frac{\partial u}{\partial x}+\frac{\partial v}{\partial y}=0 \tag{1}$$

$$u\frac{\partial u}{\partial x}+v\frac{\partial u}{\partial y}=u_\infty\frac{\partial u_\infty}{\partial x}+v\frac{\partial^2 u}{\partial y^2}+\frac{\phi\nu}{k_1}(u_\infty-u)-\frac{\sigma B^2}{\rho}(u-u_\infty) \tag{2}$$

$$u\frac{\partial T}{\partial x}+v\frac{\partial T}{\partial y}=\alpha\frac{\partial^2 T}{\partial y^2}+\tau[D_B\frac{\partial C}{\partial y}\frac{\partial T}{\partial y}+(\frac{D_T}{T_\infty})(\frac{\partial T}{\partial y})^2]-\frac{1}{(\rho C)_f}\frac{\partial q_r}{\partial y} \tag{3}$$

$$u\frac{\partial C}{\partial x}+v\frac{\partial C}{\partial y}=D_B\frac{\partial^2 C}{\partial y^2}+(\frac{D_T}{T_\infty})\frac{\partial^2 T}{\partial y^2} \tag{4}$$

with the boundary conditions

$$\begin{aligned} v=v_w, u=u_w(x)=cx, T=T_w, C=C_w \ \ at\ y=0\\ u=u_e(x)=ax, T=T_\infty, C=C_\infty \ \ as\ y\to\infty \end{aligned} \tag{5}$$

Here c is a constant such that $c>0, c<0$ for a stretching/shrinking sheet respectively, u and v are the velocity components along $x-axis$ and $y-axis$ respectively, T and C are the temperature and nanoparticle fraction of the nanofluid, ν is the kinematic viscosity of base fluid, ϕ is the volume fraction of nanoparticle, σ is the electrical conductivity of the fluid, is the constant applied magnetic field, ρ is the base fluid density, α is the thermal diffusivity, k is the thermal conductivity, $\tau=\frac{(\rho C)_p}{(\rho C)_f}$ is the ratio between $(\rho C)_p$ and $(\rho C)_f$ where $(\rho C)_f$ is the heat capacitance of the base fluid and $(\rho C)_p$ is the heat capacitance of the nanoparticles, D_B is the Brownian diffusion coefficient, D_T is the thermophoresis diffusion coefficient. It is assumed that $v_w=-\gamma(a\nu)^{\frac{1}{2}}$ is a constant mass velocity where γ is a suction parameter.

Using Roselland [31] approximations, the radiative heat flux q_r and other works are expressed as follows (Cortell [32]; Magyari & Pantokratoras [33]; Kazemi et al. [34], Waini et al. [35])

$$q_r=-\frac{4\sigma}{3k^*}\frac{\partial T^4}{\partial y} \tag{6}$$

Here σ is the Stefan-Boltzman constant and k^* is the mean absorption coefficient. Using Tayler serious expending T^4 about T_∞ while the higher-order terms are neglected, it is obtained. $T^4\approx 4T_\infty^3T-3T_\infty^3$. Following Ibrahim et al. [1], Khan and Pop [29], and Cortell [32], the following similarity variables are used:

$$\begin{aligned} \psi=(a\nu)^{\frac{1}{2}}xf(\eta), \theta(\eta)=\frac{T-T_\infty}{T_w-T_\infty}\\ \phi(\eta)=\frac{C-C_\infty}{C_w-C_\infty}, \eta=(\frac{a}{\nu})^{\frac{1}{2}}y, \end{aligned} \tag{7}$$

where ψ indicates the stream function and it is defined as $u=\frac{\partial\psi}{\partial y}$ and $v=-\frac{\partial\psi}{\partial x}$. By substituting equation (7) in equations (1),(2),(3) and (4), equation (1) is automatically satisfied and the following ODEs can be obtained:

$$f'''+ff''-f'^2+1+(K+M)(1-f')=0 \tag{8}$$

$$\frac{1}{Pr}(1+\frac{4}{3}R)\theta''+f\theta'+Nb\phi'\theta'+Nt\theta'^2=0 \tag{9}$$

$$\phi''+Lef\phi'+\frac{Nt}{Nb}\theta''=0. \tag{10}$$

Boundary conditions of (5) are reduced to

$$\begin{aligned} f(0) = \gamma, f'(0) = \lambda, \theta(0) = 1, \phi(0) = 1, \\ f'(\infty) = 1, \theta(\infty) = 0, \phi(\infty) = 0 \end{aligned} \tag{11}$$

The parameters are defined as

$$\begin{aligned} K = \frac{\phi\nu}{ak_1}, M = \frac{\sigma B^2}{\rho a}, R = \frac{4\sigma T_\infty^3}{\rho\alpha C_p k^*}, Pr = \frac{\nu}{\alpha}, Le = \frac{\nu}{D_B} \\ Nb = \frac{(\rho C)_p}{(\rho C)_f}\frac{D_B}{\nu}(C_w - C_\infty), Nt = \frac{(\rho C)_p}{\nu(\rho C)_f}(\frac{D_t}{T_\infty})(T_w - T_\infty). \end{aligned} \tag{12}$$

where Pr, Le, λ, Nb, Nt, R, M and K represent the Prandtl number, Lewis number, stretching/shrinking parameter, Brownian motion parameter, thermophoresis parameter, the thermal radiation parameter, the magnetic field parameter and the permeability parameter of the porous medium, respectively.

The primary quantities of physical interest, in this study are the skin friction coefficient C_f, the local Nusselt number Nu, and the local Sherwood number Sh which are defined as

$$C_f = \frac{\tau_w}{\rho u_\infty^2}, Nu = \frac{xq_w}{k(T_w - T_\infty)}, Sh = \frac{xq_m}{k(C_w - C_\infty)}. \tag{13}$$

here τ_w is the skin friction at the wall, q_w is the wall heat transfer by the sheet while q_m is mass heat flux. By using equation (7), we can get

$$\begin{aligned} Re_x^{\frac{1}{2}} C_f = f''(0), Re_x^{\frac{-1}{2}} Nu = [1 + \frac{4}{3}R]\theta'(0), \\ Re_x^{\frac{-1}{2}} Sh = -\phi'(0). \end{aligned} \tag{14}$$

where $Re_x = \frac{u_\infty(x)x}{\nu}$ is the local Reynolds number.

§3 Results and Discussions

The system of equations (8), (9) and (10) is solved numerically along the boundary conditions of (11) utilizing the bvp4c package in MATLAB software. The numerical results are computed for different values of the non-dimensional parameters, involved in the ODEs and similarity transformation equations. The results have been presented in tabular form and in graphic form, particularly for the suction parameter γ, the thermal radiation parameter R and magnetic parameter M. The numerical results of the skin friction coefficient $f''(0)$ obtained with different values of stretching/shrinking parameters λ are compared with the results in the literature obtained by Mahapatra and Gupta [7], Pop et al. [8] and Nazar et al. [9], and Khan and Pop [29] for the case of viscous fluid by setting $\gamma = M = K = R = 0$, in equations (8),(9) and (11).

Table 1 shows that the comparison is in a very good agreement. Therefore, the results of this study are regarded as accurate.

Generally, Table 2 and Table 3 show the values of the skin friction coefficient $f''(0)$, the local Nusselt number $-\theta'(0)$ and the local Sherwood number $-\phi'(0)$ for different values of the suction parameter γ, the magnetic field parameter M, while Table 4 show the values of the local Nusselt number $-\theta'(0)$ and the local Sherwood number $-\phi'(0)$ for different values

,

Table 1. Results comparison for skin friction coefficient $f''(0)$ for different values of the parameter λ when $\gamma = M = K = R = 0$ and Pr=1.

λ	Mahapatra and Gupta [7]	Pop et al. [8]	Nazar et al. [9]	Khan and Pop [29]	Present study
0.1	-0.9694	-0.9694	-0.9694	-0.9694	-0.9694
0.2	-0.9181	-0.9181	-0.9181	-0.9181	-0.9181
0.5	-0.6673	-0.6673	-0.6673	-0.6673	-0.6673
1	-	-	-	0	0
1.5	-	-	-	-	0.9095
2	2.0175	2.0174	2.0176	2.0175	2.0175
3	4.7293	4.729	4.7296	4.7293	4.7292
3.5	-	-	-	-	6.3006

Table 2. Results of $f''(0)$, $-\theta'(0)$ and $-\phi'(0)$ for the different values of γ when $K = 0.08, M = 0.05, Pr = 2, R = 0.3, Nb = 0.8, Nt = 0.5, Le = 3$ and $\lambda = -3.2$.

γ	$f''(0)$	$-\theta'(0)$	$-\phi'(0)$
2.2	5.623537	0.725471	4.56291
	(2.889916)	(0.526227)	(3.944007)
2.4	7.278324	0.892157	5.352447
	(1.858831)	(0.51982)	(4.287793)
2.6	8.542863	1.027691	6.034072
	(1.190033)	(0.557171)	(4.783805)

( ) dual solution

Table 3. Results of $f''(0)$, $-\theta'(0)$ and $-\phi'(0)$ for the different values of M when $K = 0.08, \gamma = 2.6, Pr = 2, R = 0.3, Nb = 0.8, Nt = 0.5, Le = 3$ and $\lambda = -3.8$.

M	$f''(0)$	$-\theta'(0)$	$-\phi'(0)$
0.02	6.623498	0.865784	5.460872
	(4.747094)	(0.765194)	(5.156971)
0.05	6.940407	0.878194	5.500128
	(4.4377)	(0.741653)	(5.091117)
0.08	7.196285	0.887653	5.530857
	(4.194227)	(0.720874)	(5.03455)

( ) dual solution

of thermal radiation parameter R, kepping the values of the Brownian parameter Nb and the thermophoresis parameter Nt, respectively. Tables 2-4 admit the existence of dual solutions in the shrinking region.

In detail, Table 2 shows that the values of $f''(0)$ are increasing as the values of γ increase in the first solution while it is decreasing in the second solution. This validates that the skin friction coefficient becomes larger as the suction becomes stronger. Table 2 also demonstrates that the variation values $-\theta'(0)$ increase for the first solution and decrease for the second solution, while the variation values of $-\phi'(0)$ increase in the first and second solutions. Table

Table 4. Results of $-\theta'(0)$ and $-\phi'(0)$ for the different values of R when $K = 0.08, \gamma = 2.6, Pr = 2, M = 0.05, Nb = 0.8, Nt = 0.5, Le = 3$ and $\lambda = -3.8$.

R	$-\theta'(0)$	$-\phi'(0)$
0	0.970116	5.362154
	(0.863291)	(4.884990)
0.3	0.878194	5.500128
	(0.741653)	(5.091117)
0.7	0.779962	5.636309
	(0.637859)	(5.264115)

( ) dual solution

3 shows that the values of $f''(0)$, $-\theta'(0)$ and $-\phi'(0)$ increase in the first solutions while the opposite trend occurs for the second solutions with the increased values of M parameter.Table 4 indicates that the skin friction coefficient $f''(0)$ is not really influenced by the thermal radiation parameter R. It is seen that the local Nusselt number $-\theta'(0)$ becomes a decreasing function for both solutions with an increase in R. Opposite trends are found for the values of the local Sherwood number $-\phi'(0)$ in both solutions when R increases.

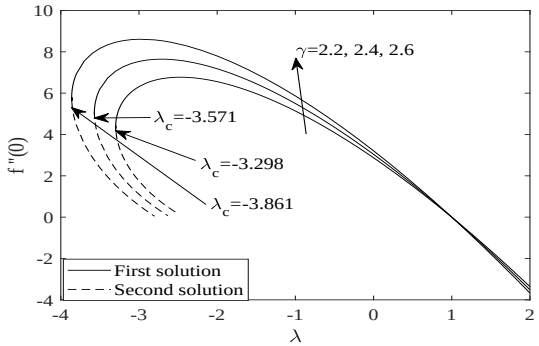

Figure 2. Variation of $f''(0)$, for the different values of γ when $K = 0.08, M = 0.05, Pr = 2, R = 0.3, Nb = 0.8, Nt = 0.5, Le = 3$.

Figures 2,3,4 show the values of $f''(0)$, $-\theta'(0)$ and $-\phi'(0)$ which represent the variations of the skin friction coefficient, the local Nusselt number and the local Sherwood number for different values of suction parameter γ. These figures admit the existence of dual solutions in a certain range of the stretching/shrinking parameter λ. There are three ranges of solutions identified from Figures 2,3,4. Dual solutions are found to exist for $\lambda_c < \lambda < \lambda_l$, unique solutions when $\lambda > \lambda_l$ and no solutions exist for $\lambda < \lambda_c$, where λ_c and λ_l are the upper and lower critical values of λ, respectively, for which ODEs (8),(9) and (10) have no solutions, where the full NavierCStokes and energy equations should be considered. The critical values λ are $\lambda_c = -3.2980$, -3.5710, -3.8610 and $\lambda_l = -2.5, -2.63, -2.8$ corresponding to the values $\gamma = 2.2, 2.4$ and 2.6, respectively. The critical value λ_c is the value where the first and second

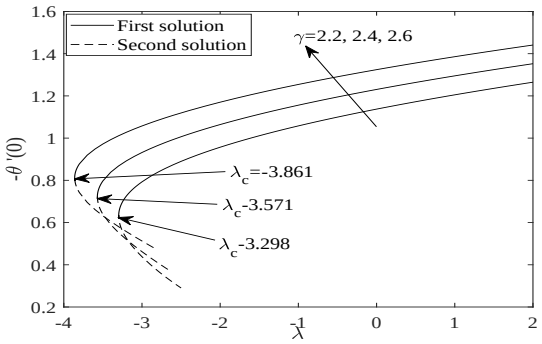

Figure 3. Variation of $-\theta'(0)$, for the different values of γ when $K = 0.08, M = 0.05, Pr = 2, R = 0.3, Nb = 0.8, Nt = 0.5, Le = 3$.

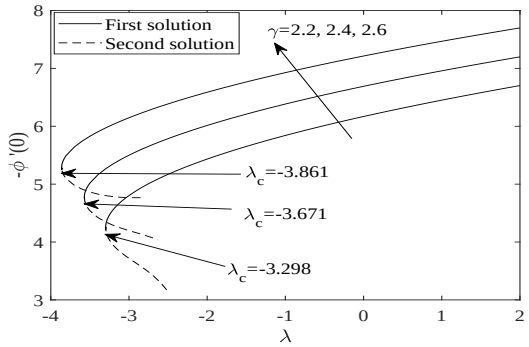

Figure 4. Variation of $-\phi'(0)$, for the different values of γ when $K = 0.08, M = 0.05, Pr = 2, R = 0.3, Nb = 0.8, Nt = 0.5, Le = 3$.

solutions are met. Figures 2,3,4 also illustrate that the critical values λ_c increase as the values of γ increase, suggesting that the suction widens the range of the dual solutions of ODEs (8),(9) and (10). Researchers like Basir et al. [36], Yan et al. [37] and Lund et al. [**?**,38] have conducted a stability analysis to determine the stable solution for a similar problem. They found that the first solution is stable, while the second solution is unstable. Based on this fact, we believe that this finding is the same for the present study and not repeated in the stability analysis here.

The values $f''(0)$ increase in the first solution, as the values γ increase, and this is depicted in figure 2. Physically, the suction leads to the reduction of the momentum boundary layer thickness, increases the surface shear stress, slows the fluid flow, and raises the velocity gradient on the surface. Figure 8 is a consistent elaboration of this.

Figure 3 shows that the values of $-\theta'(0)$ increase with the increasing γ for the first solution. The inclusion of the suction effect leads to an increase in the temperature gradient $-\theta'(0)$ and in turn increasing the local Nusselt number which represents the heat transfer rate at the surface.

Figure 4 shows the investigation of the suction effect on the local Sherwood number $-\phi'(0)$.

It is seen that the values of $-\phi'(0)$ also increase when γ increases. This situation occurs because of the suction which has decreased the concentration boundary layer thickness and consequently increased the concentration gradient $-\phi'(0)$. These findings figures 2,3,4 are supported by the values of $f''(0)$, $-\theta'(0)$ and $-\phi'(0)$ presented in Table 2.

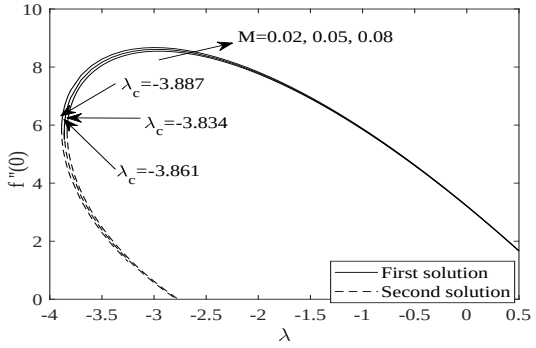

Figure 5. Variation of $f''(0)$, for the different values of M when $K = 0.08, \gamma = 2.6, Pr = 2, R = 0.3, Nb = 0.8, Nt = 0.5, Le = 3$.

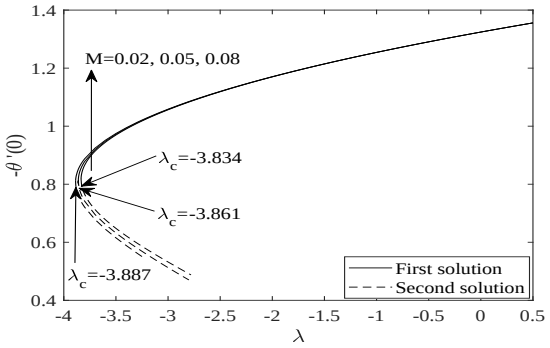

Figure 6. Variation of $-\theta'(0)$, for the different values of M when $K = 0.08, \gamma = 2.6, Pr = 2, R = 0.3, Nb = 0.8, Nt = 0.5, Le = 3$.

Figures 5,6,7 show the variations of $f''(0)$, $-\theta'(0)$ and $-\phi'(0)$ for different values of M. Dual solutions exist for a certain range of $\lambda_c < \lambda < \lambda_l$, a unique solution when $\lambda = \lambda_c$ and $\lambda > \lambda_l$ and no solution for $\lambda < \lambda_c$. The critical values $\lambda_c = -3.8341, -3.8610, -3.8871$ and $\lambda_l = -2.75, -2.8, -3.25$ correspond to the values of $M = 0.02, 0.04$ and 0.08, respectively.

The variations of $f''(0)$, $-\theta'(0)$ and $-\phi'(0)$, are increased in the first solution while decreasing in the second solution as the values of M increase. Similar to the suction effect, it is also observed that the critical values λ_c also increase as the values of M increase. This finding proposes that the magnetic field effect expands the range of the dual solutions of Eqns. (8)-(10) that exist.

In Figure 5, the values of $f''(0)$ increase in the first solutions as the values γ increase while

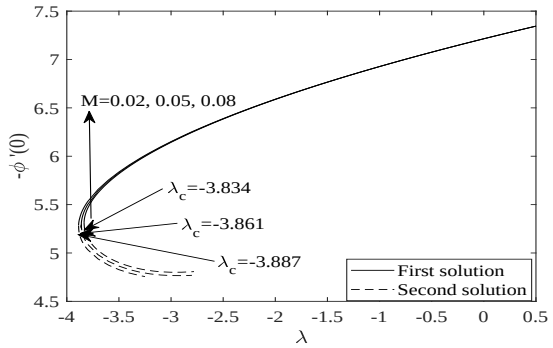

Figure 7. Variation of $-\phi'(0)$, for the different values of M when $K = 0.08, \gamma = 2.6, Pr = 2, R = 0.3, Nb = 0.8, Nt = 0.5, Le = 3$.

the opposite behavior is shown for the second solutions. As the strength of the magnetic field becomes stronger, the Lorentz force generates resistance force to the fluid motion and hence decreases the fluid velocity which is consistent with the velocity profile in figure 11. As a result, the momentum boundary thickness decreases, further increasing the velocity gradient $f''(0)$ at the surface.

Figure 6 exhibits the magnetic field impact on the values of $-\theta'(0)$. Again, M has increased the heat transfer rate at the surface for the first solution while it is the other way around for the second solution. This trend occurs due to the fact that Lorentz force decreases the temperature of the nanofluid which can be seen in figure 12 and in turn increases the temperature gradient $-\theta'(0)$ at the surface.

Similar behavior also occurs for the variations of $-\phi'(0)$. The values of $-\phi'(0)$ are found to be increased only for the first solution as illustrated in figure 7. This finding is obtained because the magnetic field effect has decreased the concentration boundary layer thickness and in turn increased the concentration gradient $-\phi'(0)$.

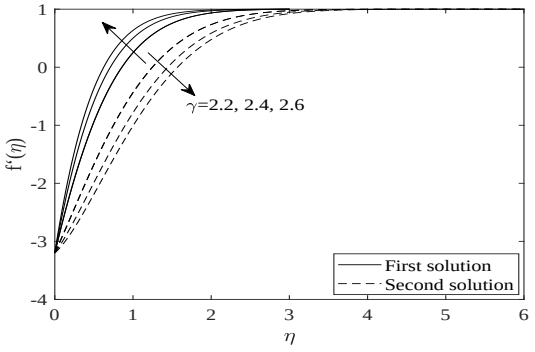

Figure 8. The velocity profile $f'(\eta)$, for the different values of γ when $K = 0.08, M = 0.05, Pr = 2, R = 0.3, Nb = 0.8, Nt = 0.5, Le = 3$ *and* $\lambda = -3.2(shrinking\ case)$.

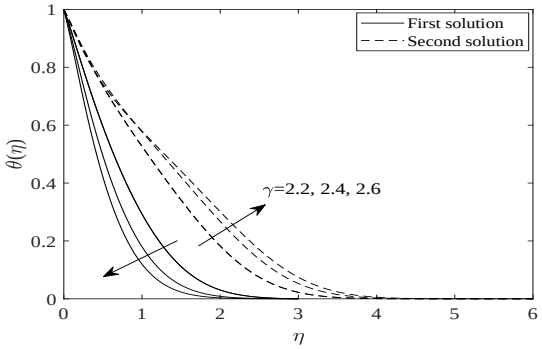

Figure 9. The temperature profile $\theta(\eta)$, for the different values of γ when $K = 0.08, M = 0.05, Pr = 2, R = 0.3, Nb = 0.8, Nt = 0.5, Le = 3$ *and* $\lambda = -3.2(shrinking\ case)$.

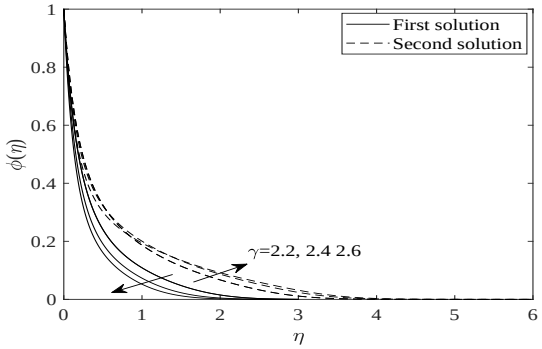

Figure 10. The concentration profile $\phi(\eta)$, for the different values of γ when $K = 0.08, M = 0.05, Pr = 2, R = 0.3, Nb = 0.8, Nt = 0.5, Le = 3$ *and* $\lambda = -3.2(shrinking\ case)$.

Figures 8,9,10 are sketched to know the effect of the suction on the fluid velocity of nanofluid $f'(\eta)$, fluid temperature $\theta(\eta)$ and fluid concentration $\phi(\eta)$ in the shrinking case. It is clear that from figure 8, the fluid velocity decreases with an increase in γ for the first solution. As the suction parameter increases, it causes the reduction in the momentum boundary layer thickness and the decrease in the nanofluid motion. The physical implication of suction is as suction enhances the heated fluid flow is flowing towards the boundary of the sheet. Therefore, it becomes cause to decelerate the fluid flow and enhances the velocity. Ultimately the temperature of the fluid flow is decreasing because the flow of fluid towards the sheet boundary makes thin of the boundary layer in.

On the other hand, the fluid temperature is found to be decreased for the first solution with the increasing suction strength in flow as shown in figure 9. In the physical aspect, the suction effect causes the reduction in the thermal boundary layer thickness and reduces the nanofluid temperature. The observation happens for fluid concentration $\phi(\eta)$ where it is decreased with the increasing suction strength as sketched in figure 10. This finding is obtained due to the

reduction in the concentration boundary layer thickness as the suction effect increases.

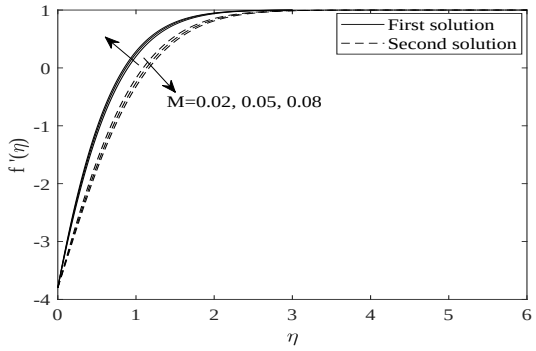

Figure 11. The velocity profile $f'(\eta)$, for the different values of M when $K = 0.08, \gamma = 2.6, Pr = 2, R = 0.3, Nb = 0.8, Nt = 0.5, Le = 3$ *and* $\lambda = -3.8(shrinking\ case)$.

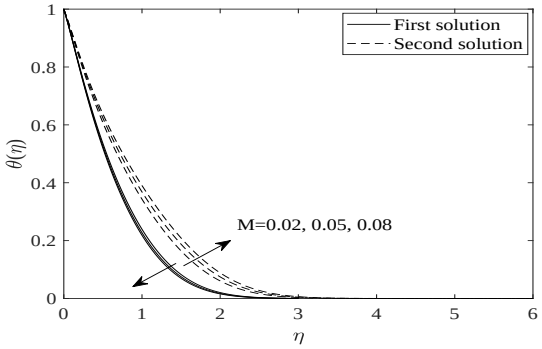

Figure 12. The temperature profile $\theta(\eta)$, for the different values of M when $K = 0.08, \gamma = 2.6, Pr = 2, R = 0.3, Nb = 0.8, Nt = 0.5, Le = 3$ *and* $\lambda = -3.8(shrinking\ case)$.

Figures 11,12,13 show the velocity profile, temperature profile, and concentration profile for different values of M with other parameters fixed in the shrinking case. As M increases, the nanofluid velocity $f'(\eta)$ decreases in the first solution which causes the reduction in the momentum boundary layer thickness, increases the temperature gradient at the surface and in turn enhances the heat transfer rate at the surface.

In figure 12 and 13, it is observed that both the fluid temperature $\theta(\eta)$ and fluid concentration $\phi(\eta)$ are decreased in the first solutions, respectively. This finding occurs because of the decreasing thermal and concentration boundary layer thickness in the increase in M.

The effect of the thermal radiation parameter R on local Nusselt number is illustrated in figure 14. The variation of local Nusselt number (heat transfer rate) is decreasing as the values of increase in both the first and second solutions. Physically, greater values of R generate additional heat to the nanofluid which shows an increment in the temperature as can be seen in figure 15. The critical values $\lambda_c = -3.860, -3.861, -3.861$ and $\lambda_l = -2.79, -2.8, -2.9$

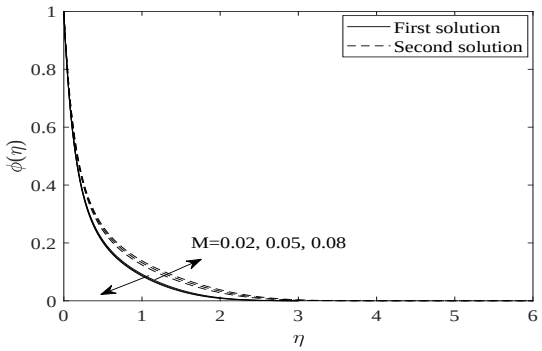

Figure 13. The concentration profile $\phi(\eta)$, for the different values of M when $K = 0.08, \gamma = 2.6, Pr = 2, R = 0.3, Nb = 0.8, Nt = 0.5, Le = 3$ *and* $\lambda = -3.8(shrinking\ case)$.

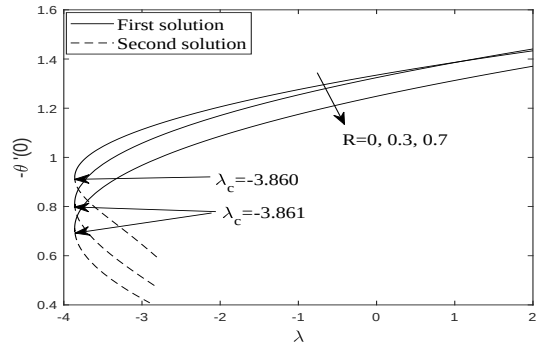

Figure 14. Variation of $-\theta'(0)$, for the different values of R when $K = 0.08, \gamma = 2.6, Pr = 2, M = 0.05, Nb = 0.8, Nt = 0.5, Le = 3$.

correspond to the values of $R = 0, 0.3$ and 0.7, respectively. The velocity profiles for different R are not sketched here because gave no impact on the skin friction coefficient as can been seen in ODEs eqns. (8)-(9).

Figure 15 depicts that as R increases, the temperature also increases for both the first and second solutions. Practically, an increase in the thermal radiation parameter has caused the increase in the thermal boundary layer thickness. As a result, the heat transfer rate at the surface decreases. Basically, the thermal radiation works as a heat source, and due to this the quantity of heat added to the fluid is increased. This is the reason why the nanofluid temperature increases and as the consequence the heat transfer rate decreases.

Figure 16 shows the effect of the thermal radiation parameter on the local Sherwood number which represents the mass heat flux rate. It is observed that the values of the mass heat flux rate increase for both the first and second solutions as the values of R increase. Physically, as the thermal radiation parameter increases, the concentration boundary layer thickness decreases while the wall concentration gradient increases.

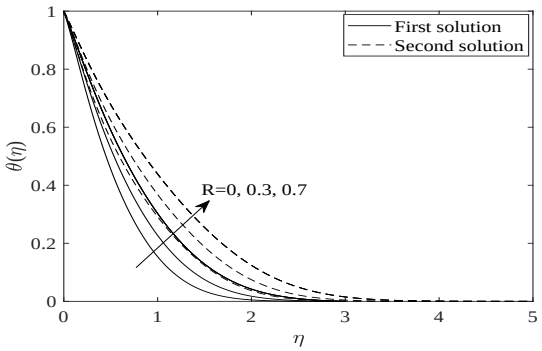

Figure 15. The temperature profile $\theta(\eta)$, for the different values of R when $K = 0.08, \gamma = 2.6, Pr = 2, M = 0.05, Nb = 0.8, Nt = 0.5, Le = 3$ *and* $\lambda = -3.8$(*shrinking case*).

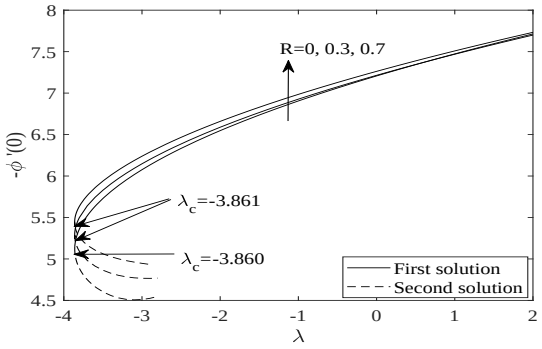

Figure 16. Variation of $-\phi'(0)$, for the different values of R when $K = 0.08, \gamma = 2.6, Pr = 2, M = 0.05, Nb = 0.8, Nt = 0.5, Le = 3$.

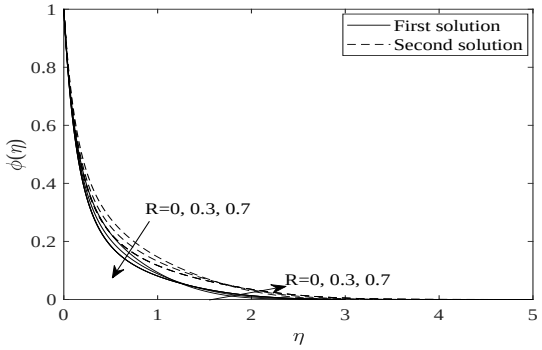

Figure 17. The concentration profile $\phi(\eta)$, for the different values of R when $K = 0.08, \gamma = 2.6, Pr = 2, M = 0.05, Nb = 0.8, Nt = 0.5, Le = 3$ *and* $\lambda = -3.8$(*shrinking case*).

Figure 17 illustrates the concentration profile for some values of R and it depicts that the fluid concentration decreases as the values increase, and hence the findings in Fig. 16 are

supported.

§4 Conclusions

The current study analyzes the effect of the suction on MHD boundary layer stagnation point flow of a nanofluid through a stretching/shrinking sheet. The system of nonlinear PDEs described in the problem is transformed into ODEs using similarity transformation. The ODEs were solved using the bvp4c technique in MATLAB software numerically. A comparison of the present results with previously published works has been done for a specific case and an excellent agreement is found between both results. Brief numerical results for the profiles of velocity, temperature and concentration as well as the skin friction coefficient, the local Nusselt number and the local Sherwood number are presented in tabular and graphical forms. The numerical solution obtained depends on several governing parameters namely the suction, magnetic field, thermal radiation, and the stretching/shrinking parameters. Dual solutions exist for a certain range of suction and stretching/shrinking parameters. Furthermore, it is found that the skin friction coefficient, the local Nusselt number and the local Sherwood number are increased with the increasing suction parameter. An increase in the magnetic field effect causes the values of the skin friction coefficient, Nusselt number, and Sherwood number to increase due to Lorentz force or drag force of flow. It is also observed that when the values of the thermal radiation parameter increase, the local Nusselt number is decreased and the Sherwood number is increased, respectively.

The following key points are included in conclusion

1. Dual solutions exist for $\lambda > \lambda_c$.

2. M causes a substantial increase in the surface heat transfer rate. Physically decreases boundary layer thickness.

3. Increasing the mass suction causes to decrease the momentum boundary layer thickness and temperature.

4. The rate of heat transfer decreases with a rise of R thats why temperature increases.

Declarations

Conflict of interest The authors declare no conflict of interest.

References

[1] W Ibrahim, B Shankar, M M Nandeppanavar. *MHD stagnation point flow and heat transfer due to nanofluid towards a stretching sheet*, Int J Heat Mass Transf, 2013, 56: 1-9.

[2] B C Sakiadis. *Boundary layer behaviour on continuous solid surfaces, II. The boundary layer on a continuous flat surface*, A I Ch E J, 1961, 7(1): 221-225.

[3] L J Crane. *Flow past a stretching plate*, J Appl Math Phys, 1970, 21(3): 645-647.

[4] A Ishak, J H Merkin, R Nazar, I Pop. *Mixed convection boundary layer flow over a permeable vertical surface with prescribed wall heat flux*, Z Angew Math Phys, 2008, 59: 100-123.

[5] F Kamal, K Zaimi, A Ishak, I Pop. *Stability analysis of MHD stagnation-point flow towards a permeable stretching/ shrinking sheet in a nanofluid with chemical reactions effect*, Sains Malaysiana, 2019, 48(1): 243-250.

[6] K Hiemenz. *Die grenzschicht an einem in den gleichformigen flussigkeitsstrom eingetauchten geraden kreiszlynder*, Dingler Polytech J, 1911, 326: 321-340.

[7] T R Mahapatra, A S Gupta. *Heat transfer in stagnation-point flow towards a stretching sheet*, Heat Mass Transf, 2002, 38(6): 517-521.

[8] S R Pop, T Grosan, I Pop. *Radiation effects on the flow near the stagnation point of a stretching sheet*, Tech Mech, 2004, 25: 100-106.

[9] R Nazar, N Amin, D Filip, I Pop. *Stagnation point flow of a micropolar fluid towards a stretching sheet*, Int J Non Linear Mech, 2004, 39(7): 1227-1235.

[10] R A Hamid, N A A Bakar, K Zaimi, B Bidin. *MHD mixed convection stagnation point flow over a permeable surface*, AIP Conf Proc, 2013, 1522(470): 470-475.

[11] U Yashkun, K Zaimi, N A A Bakar, M Ferdows. *Nanofluid stagnation-point flow using Tiwari and Das model over a stretching/shrinking sheet with suction and slip effects*, Journal of Advanced Research in Fluid Mechanics and Thermal Sciences, 2020, 70(1): 62-76.

[12] A Tassaddiq, I Khan, K Sooppy Nisar, J Singh. *MHD flow of a generalized Casson fluid with Newtonian heating: A fractional model with MittagCLeffler memory*, Alexandria Eng J, 2020, 59(5): 3049-3059.

[13] K S Nisar, U Khan, A Zaib, I Khan, D Baleanu. *Numerical Simulation of Mixed Convection Squeezing Flow of a Hybrid Nanofluid Containing Magnetized Ferroparticles in 50%:50% of Ethylene GlycolCWater Mixture Base Fluids Between Two Disks With the Presence of a Non-linear Thermal Radiation Heat Flux*, Front Chem, 2020, 8: 1-12.

[14] L A Lund, Z Omar, S Dero, I Khan, D Baleanu, K S Nisar. *Magnetized Flow of Cu + Al2O3 + H2O Hybrid Nanofluid in Porous Medium: Analysis of Duality and Stability*, Symmetry (Basel), 2020, 12(9): 1513.

[15] T Anwar, P Kumam, Asifa, I Khan, P Thounthong. *Generalized Unsteady MHD Natural Convective Flow of Jeffery Model with ramped wall velocity and Newtonian heating; A Caputo-Fabrizio Approach*, Chinese J Phys, 2020, 68: 849-865.

[16] M Hamid, M Usman, Z H Khan, R Ahmad, W Wang. *Dual solutions and stability analysis of flow and heat transfer of Casson fluid over a stretching sheet*, Phys Lett Sect A Gen At Solid State Phys, 2019, 383(20): 2400-2408.

[17] N A Sheikh, D L C Ching, I Khan, D Kumar, K S Nisar. *A new model of fractional Casson fluid based on generalized Ficks and Fouriers laws together with heat and mass transfer*, Alexandria Eng J, 2020, 59(5): 2865-2876.

[18] S U S Choi. *Enhancing Thermal Conductivity of Fluids with Nanoparticles, In: D. A. Siginer and H. P. Wang, Eds., Developments and Applications of Non-Newtonian Flows*, ASME, New York, 1995, 66: 99-105.

[19] C A Reddy, B Shankar. *Magnetohydrodynamics stagnation point flow of a nano fluid over an exponentially stretching sheet with an effect of chemical reaction , heat source and suction / injunction*, World J Mech, 2015, 5: 211-221.

[20] M K Chaudhary, S Chaudhary, R Sharma. *Unsteady MHD flow and heat transfer over a stretching permeable surface with suction or injection*, Procedia Eng, 2015, 127: 703-710.

[21] A Ishak, K Jafar, R Nazar, I Pop. *MHD stagnation point flow towards a stretching sheet*, Phys A Stat Mech its Appl, 2009, 388(17): 3377-3383.

[22] I J Uwanta and M M Hamza. *Effect of suction / injection on unsteady hydromagnetic convective flow of reactive viscous fluid between vertical porous plates with thermal diffusion*, Int Sch Res Not, 2014, 2014, Article ID: 980270.

[23] L A Lund, Z Omar, S Dero, D Baleanu, I Khan. *Rotating 3d flow of hybrid nanofluid on exponentially shrinking sheet: Symmetrical solution and duality*, Symmetry, 2020, 12(10): 1-14.

[24] L A Lund, Z Omar, S Dero, I Khan, D Baleanu, K S Nisar. *Magnetized Flow of Cu + Al2O3 + H2O Hybrid Nanofluid in Porous Medium: Analysis of Duality and Stability*, Symmetry (Basel), 2020, 12(9): 1513, DOI: 10.3390/sym12091513.

[25] L A Lund, Z Omar, S Dero, Y Chu, I Khan, K S Nisar. *Temporal stability analysis of magnetized hybrid nanofluid propagating through an unsteady shrinking sheet: Partial slip conditions*, Computers, Materials and Continua, 2020, 66(2): 1963-1975.

[26] A M Rohni. *Multiple Similarity Solutions of Steady and Unstedy Convection Boundary Layer Flows in Viscous Fluids and Nanofluids*, Universiti Sains Malaysia, 2013.

[27] S Dero, A M Rohni, A Saaban, I Khan. *Dual Solutions and Stability Analysis of Micropolar Nanofluid Flow with Slip E ect on Stretching/Shrinking Surfaces*, Energies, 2019, 12(4529).

[28] N S Khashiie, N M Arifin, R Nazar, E H Hafidzuddin, N Wahi, I Pop. *Mixed convective flow and heat transfer of a dual stratified micropolar fluid induced by a permeable stretching/shrinking sheet*, Entropy, 2019, 21(12): 1-16.

[29] W A Khan, I Pop. *Boundary-layer stagnation-point flow toward a stretching surface in a porous nanofluid-filled medium*, J Thermophys Heat Transf, 2012, 26(1): 147-153.

[30] D A Nield, A V Kuznetsov. *The Cheng-Minkowycz problem for natural convective boundary-layer flow in a porous medium saturated by a nanofluid*, Int J Heat Mass Transf, 2009, 52: 5792-5795.

[31] S Roselland. *Astrophysik Und Atom-Theoretische Grundlagen*, Springer-Verlag, Berlin, 1931, 41-44.

[32] R Cortell. *Flow and heat transfer of a fluid through a porous medium over a stretching surface with internal heat generation/absorption and suction/blowing*, Fluid Dyn Res, 2005, 37(4): 231-245.

[33] E Magyari, A Pantokratoras. *Note on the effect of thermal radiation in the linearized rosseland approximation on the heat transfer characteristics of various boundary layer flows*, International Communications in Heat and Mass Transfer, 2011, 38(5): 554-556.

[34] M A Kazemi, S S Jafari, S M Musavi, M Nejati. *Analytical solution of convective heat transfer of a quiescent fluid over a nonlinearly stretching surface using homotopy analysis method*, Results in Physics, 2018, 10(2018): 164-172.

[35] I Waini, A Ishak, I Pop. *Hybrid nanofluid flow and heat transfer over a nonlinear permeable stretching/shrinking surface*, Int J Numer Methods Heat Fluid Flow, 2019, 29(9): 3110-3127.

[36] M F M Basir, M E H Hafidzuddin, K Naganthran, Hashim, S S Chaharborj, M S M Kasihmuddin, R Nazar. *Stability analysis of unsteady stagnation-point gyrotactic bioconvection flow and heat transfer towards the moving sheet in a nanofluid*, Chinese Journal of Physics, 2020, 65(2020): 538-553.

[37] L Yan, S Dero, I Khan, I A Mari, D Baleanu, K S Nisar, E S M Sherif, H S Abdo. *Dual solutions and stability analysis of magnetized hybrid nanofluid with joule heating and multiple slip conditions*, Processes, 2020, 8(3): 332.

[38] L A Lund, Z Omar, I Khan, E S M Sherif. *Dual solutions and stability analysis of a hybrid nanofluid over a stretching/shrinking sheet executing MHD flow*, Symmetry, 2020, 12(2): 276.

[39] L A Lund, Z Omar, Z I Khan, A H Seikh, E S M Sherif, K S Nisar. *Stability analysis and multiple solution of Cu-Al2O3/H2O nanofluid contains hybrid nanomaterials over a shrinking surface in the presence of viscous dissipation*, Journal of Materials Research and Technology, 2020, 9(1): 421-432.

[1]Centre of Excellence for Social Innovation and Sustainability, Institute of Engineering, Universiti Malaysia Perlis, Pauh Putra Campus, 02600, Arau, Perlis, Malaysia.

[2]Department of Mathematics, Sukkur IBA University, Airport Road, Sukkur, 65200, Sindh, Pakistan.
[3]Department of Mathematics and Statistics, Faculty of Applied Sciences and Technology, Universiti Tun Hussein Onn Malaysia, Johor, Malaysia.
[4]Department of Mathematics, Faculty of Science, New Valley University, Al-Wadi Al-Gadid, Al-Kharga 72511, Egypt.
[5]Mathematics Department, Faculty of Science, Northern Border University, Arar 1321, Saudi Arabia.
[6]Research Group of Fluid Flow Modeling and Simulation, Department of Applied Mathematics, University of Dhaka, Dhaka-1000, Bangladesh.
Email: khairy@unimap.edu.my